To be submitted to ApJ

Our Sun. V. A Bright Young Sun Consistent with Helioseismology and Warm Temperatures on Ancient Earth and Mars

I.-Juliana Sackmann and Arnold I. Boothroyd[1]

W. K. Kellogg Radiation Laboratory 106-38, California Institute of Technology, Pasadena, CA 91125

ijs@krl.caltech.edu

aib@krl.caltech.edu

ABSTRACT

The relatively warm temperatures required on early Earth and Mars have been difficult to account for with warming from greenhouse gases. A slightly more massive young Sun would be brighter than predicted by the standard solar model, simultaneously resolving this problem for both Earth and Mars. We computed high-precision solar models with seven initial masses, from $M_i = 1.01$ to 1.07 $M_\odot$ — the latter being the maximum permitted if the early Earth is not to lose its water via a moist greenhouse effect. The relatively modest early mass loss that is required remains consistent with observational limits on mass loss from young stars and with estimates of the past solar wind obtained from lunar rocks. We considered three types of mass loss rates: (i) a reasonable choice of a simple exponential decline, (ii) an extreme step-function case that gives the maximum effect consistent with observations, and (iii) the radical case of a linear decline which is inconsistent with the solar wind mass loss estimates from lunar rocks. Our computations demonstrated that mass loss leaves a fingerprint on the Sun's internal structure large enough to be detectable with helioseismic observations. All of our mass-losing solar models were consistent with the helioseismic observations; in fact, our preferred mass-losing cases were in marginally better agreement with the helioseismology than the standard solar model was, although this difference was smaller than the effects of other uncertainties in the

[1]Present address: CITA, U. of Toronto, 60 St. George Street, Toronto, Ontario, Canada M5S 3H8; boothroy@cita.utoronto.ca

input physics and in the solar composition. Mass loss has only a relatively minor effect on the predicted lithium depletion; the major portion of the solar lithium depletion must still be due to rotational mixing. Thus the modest mass loss cases considered here cannot be ruled out by observed lithium depletions. For the three mass loss types considered, the preferred initial masses were 1.07 $M_\odot$ for the exponential case and 1.04 $M_\odot$ for the step-function and linear cases; all of these provided high enough solar fluxes at Mars 3.8 Gyr ago to be consistent with the existence of liquid water. For a more massive early Sun, the planets would have had to be closer to the young Sun in order to end up in their present orbits (e.g., 7% and 4% closer at birth for our preferred cases); the orbital radii of the planets would vary inversely with the solar mass. Both of these effects contribute to the fact that the early solar flux at the planets would have been considerably higher than that of the standard solar model at that time — e.g., for our preferred initial masses, 30 to 50% higher at birth than the standard model predicts, and 10 to 20% higher 3.8 Gyr ago than the standard model at that epoch. In fact, the 1.07 $M_\odot$ exponential case has a flux at birth 5% higher than the present solar flux, while the radical 1.04 $M_\odot$ linear case has a nearly constant flux over the first 3 Gyr only about 10% lower than at present. The early solar evolution would be in the opposite direction in the H-R diagram to that of the standard Sun.

Subject headings: Sun: evolution — Sun: helioseismology — Sun: solar-terrestrial relations — Sun: solar wind — planets and satellites: individual (Earth, Mars)

1. Introduction

Observations indicate that the Earth was at least warm enough for liquid water to exist as far back as 4 Gyr ago, namely, as early as half a billion years after the formation of the Earth (Cogley & Henderson-Sellers 1984; Mojzsis et al. 1996; Eiler, Mojzsis, & Arrhenius 1997; Eriksson 1982; Bowring, Williams, & Compston 1989; Nutman et al. 1984); in fact, there is evidence suggesting that Earth may have been even warmer then than it is now (Kasting 1989; Oberbeck, Marshall, & Aggarwal 1993; Woese 1987; Ohmotu & Felder 1987; Knauth & Epstein 1976; Karhu & Epstein 1986). These relatively warm temperatures required on early Earth are in apparent contradiction to the dimness of the early Sun predicted by the standard solar models. This problem has generally been explained by assuming that Earth's early atmosphere contained huge amounts of carbon dioxide (CO_2), resulting in a large enough greenhouse effect to counteract the effect of a dimmer Sun. However, the re-

cent work of Rye, Kuo, & Holland (1995) places an upper limit of 0.04 bar on the partial pressure of CO_2 in the period from 2.75 to 2.2 Gyr ago, based on the absence of siderite in paleosols; this casts doubt on the viability of a strong CO_2 greenhouse effect on early Earth. The existence of liquid water on early Mars has been even more of a puzzle; even the maximum possible CO_2 greenhouse effect cannot yield warm enough Martian surface temperatures (Kasting 1991; Kasting, Whitmire, & Reynolds 1993). These problems can simultaneously be resolved, for both Earth and Mars, if the early Sun were brighter than predicted by the standard solar models. This could be accomplished if the early Sun were slightly more massive than it is now.

Helioseismic observations provide revolutionary precision for probing the solar interior. Helioseismic frequencies are observed with an accuracy of a few parts in 10^5, allowing measurement of the sound speed profile throughout most of the Sun's interior to an accuracy of a few parts in 10^4 (Basu, Pinsonneault, & Bahcall 2000). This high precision permits one to search for subtle effects in the interior structure of the present Sun resulting from events in the distant past. In particular, modest mass loss (between 1% and 7% of the Sun's mass) early on the main sequence might have left enough of a fingerprint on the interior structure of the present Sun to be detectable by helioseismological observations.

1.1. Limits On Early Solar Mass Loss

Willson, Bowen, & Struck-Marcel (1987) first presented the hypothesis that stars like the Sun might lose significant amounts of mass on the early main sequence. Guzik, Willson, & Brunish (1987) were the first to compute solar models with such early main sequence mass loss, namely, an extreme case with an initial mass of 2 $M_\odot$. Such extreme mass loss (of $\Delta M = 1\ M_\odot$) turns out to be unrealistic, as discussed below; but small mass loss cases cannot be ruled out at the present. Boothroyd, Sackmann, & Fowler (1991) considered an initial solar mass of 1.1 $M_\odot$, showing that this is the upper limit allowed by the observed solar lithium depletion. Guzik & Cox (1995) considered initial solar masses of 1.1 and 2 $M_\odot$, concluding that the 2 $M_\odot$ could be ruled out by helioseismic observations, and that for the 1.1 $M_\odot$ case a mass loss timescale of 0.2 Gyr was favored over a 0.45 Gyr timescale. Morel, Provost, & Berthomieu (1997) also used helioseismology to test an initial solar mass of 1.1 $M_\odot$, finding that a short mass loss timescale of 0.2 Gyr had essentially no effect, while a longer timescale of 0.45 Gyr had a significant effect (slightly worsening the agreement of their models with the helioseismic observations).

Presently, the Sun is experiencing only a negligible amount of mass loss: the solar wind removes mass at a rate $\sim 3 \times 10^{-14}\ M_\odot\ \mathrm{yr}^{-1}$. If this mass loss rate had been constant over

the last 4.5 Gyr, the young Sun would have been more massive by only $\sim 10^{-4}\ M_\odot$. The contemporary solar wind has been observed only for three decades, and has been found to be a highly variable phenomenon — all properties, including flux, velocity, and composition vary significantly (Geiss & Bochsler 1991). The lunar surface material carries the signature of the solar wind irradiation over the past several Gyr; measurements of noble gas isotopes in lunar samples suggest that the average solar wind flux over the past ~ 3 Gyr was an order of magnitude higher than it is today (Geiss 1973; Geiss & Bochsler 1991; Kerridge et al. 1991). This implies a total solar mass loss of $\sim 10^{-3}\ M_\odot$ over the past 3 to 4 Gyr (the age of the oldest available lunar material). Some older, solar-flare irradiated grains from meteorites imply an early solar flare activity about 10^3 times that of the present Sun (Caffee, Hohenberg, & Swindle 1987); the associated solar wind may have been enhanced by a similar factor of $\sim 10^3$, most likely during the first ~ 1 Gyr of the Sun's life on the main sequence (Whitmire et al. 1995), implying a total mass loss during this first 1 Gyr period of as much as $\sim 0.03\ M_\odot$ (if the average mass loss rate throughout that period was indeed $\sim 10^3$ times the present rate of $3 \times 10^{-14}\ M_\odot \mathrm{yr}^{-1}$). Such a change in the solar mass would be sufficient to cause a significant increase in the luminosity of the young Sun.

Since the Sun is a typical main sequence star, it is reasonable to assume that mass loss rates in the young Sun would be similar to those in other young solar-type main sequence stars. There have been several attempts to measure mass loss in early main sequence stars. It is observationally a very challenging task. Brown et al. (1990) attempted to obtain mass loss rates for 17 young main sequence stars somewhat hotter and more massive than the Sun (A and F dwarfs), finding upper limits to the mass loss rates of 10^{-10} to $10^{-9}\ M_\odot$/yr; these limits are even less constraining than the highest solar mass loss rate suggested by the meteoritic and lunar data. Gaidos, Güdel, & Blake (2000) used 3.6 cm VLA observations to place more stringent upper limits of $\dot{M} \lesssim 5 \times 10^{-11}\ M_\odot\ \mathrm{yr}^{-1}$ on mass loss rates of three young main sequence stars of roughly solar mass (π^{01} UMa, κ^1 Cet, and β Com) — as discussed in § 2.1, an initial solar mass of $1.07\ M_\odot$ would require early solar mass loss rates that are only marginally consistent with these limits. Wood et al. (2001) recently used HST observations of H I Lyα absorption to measure the stellar wind from the sun-like star α Cen (which is not, however, a young star), finding a mass loss rate roughly twice as large as that of the Sun; they also find an upper limit roughly ten times lower for its cooler, less massive companion Proxima Cen. A similar method had earlier been used by Wood & Linsky (1998) to look at four other main sequence stars cooler and less massive than the Sun (finding stellar winds of roughly the same order of magnitude as the solar wind). Such a method applied to young, Sun-like stars holds promise for placing stringent limits on early main sequence mass loss.

The observed depletion of lithium in the Sun provides a stringent upper limit to the total solar mass loss of $\Delta M \sim 0.1\ M_\odot$; i.e., the initial solar mass M_i (4.5 Gyr ago) is constrained

to be $M_i \lesssim 1.1\ M_\odot$ (Boothroyd et al. 1991). However, this is much too generous an upper limit. There are additional mechanisms that can deplete solar lithium. One mechanism, namely, pre-main-sequence lithium depletion (during the Sun's initial contraction phase), was taken into account in our mass-losing solar models (for the Sun, this depletion was a factor of ~ 20, as discussed below and in our companion paper "Our Sun IV" [Boothroyd & Sackmann 2001]). Another mechanism is rotation-induced turbulent mixing, which probably is the major cause of the main-sequence lithium depletion; however, rotation models have free parameters, and can be fitted to *any* required amount of solar lithium depletion (see, e.g., Schatzman 1977; Lebreton & Maeder 1987; Pinsonneault et al. 1989; Richard et al. 1996). Also, it has been shown that mass loss cannot be the major contributor to the observed lithium depletions in the young Hyades cluster (Swenson & Faulkner 1992); these lithium depletions might possibly be accounted for by standard pre-main-sequence depletion alone, if the Hyades oxygen abundance were substantially higher than the canonical value (Swenson et al. 1994). While pre-main-sequence depletion might account for much (or even all) of the Hyades lithium depletion, it cannot account for more than a fraction of the lithium depletion observed in older and less metal-rich stars, such as the Sun and the stars in clusters such as NGC 752, M67, or NGC 188 (see, e.g., Hobbs & Pilachowski 1988; Balachandran 1995). These stars are observed to have a total lithium depletion much *larger* than that of Hyades stars of the same mass, but they would have experienced *less* pre-main-sequence lithium depletion, due to their lower metallicity.

An even more stringent upper limit to the Sun's initial mass is imposed by the requirement that the early Earth not lose its water via a *moist greenhouse effect*, which would occur if the solar flux at Earth were more than 10% higher than its present value (Kasting 1988) — a moist greenhouse occurs when the stratosphere becomes wet, and H_2O is lost through UV dissociation and the subsequent loss of hydrogen to space. This solar flux limit corresponds to an upper limit on the Sun's initial mass of $M_i \lesssim 1.07\ M_\odot$, which is the most stringent upper limit on the Sun's initial mass.

The only strong lower limit on M_i comes from the fact that the Sun is converting matter into energy and radiating it away; $\Delta E = L\Delta t = \Delta M c^2$, where ΔE is the total energy radiated away, L is the average solar luminosity (including the neutrino luminosity) Δt is the ~ 4.5 Gyr duration of the nuclear burning, ΔM is the amount of mass converted into energy, and c is the speed of light (note that elsewhere in the paper we use "c" to denote the adiabatic sound speed). At present, mass is radiated away as photons and neutrinos at a rate slightly over twice the solar wind mass loss rate. For the standard solar model, the Sun's average luminosity over the last 4.5 Gyr was about 0.85 times its present luminosity. It follows that $\Delta M \approx 3 \times 10^{-4}\ M_\odot$ from radiation losses alone (i.e., that $M_i \gtrsim 1.0003\ M_\odot$). Such a minor amount of mass loss has a negligible effect on the early solar luminosity.

There are also considerations that put soft lower limits on the Sun's initial mass M_i. If the present observed solar wind rate of $\sim 3 \times 10^{-14}\ M_\odot$/yr had been constant over the Sun's history, the total amount of solar wind mass loss would have been only $\sim 1.4 \times 10^{-4}\ M_\odot$; including the $\Delta M \approx 3 \times 10^{-4}\ M_\odot$ from radiation losses would imply $M_i \sim 1.0004\ M_\odot$. However, measurements of the noble gases implanted in lunar samples suggest an average solar wind flux over the past ~ 3 Gyr an order of magnitude higher than at present, (Geiss 1973; Geiss & Bochsler 1991; Kerridge et al. 1991), implying a total solar mass loss over that period of $\sim 0.001\ M_\odot$, i.e., a solar mass 3 Gyr ago of $M(-3\,\mathrm{Gyr}) \sim 1.001\ M_\odot$ — note that $M(-t)$ is used to refer to the solar mass at t years before the present. The ~ 3 Gyr age of these lunar rocks means that they place no limits on *earlier* solar mass loss, so that all one can say is that $M_i \geq M(-3\,\mathrm{Gyr})$. Older, solar-flare irradiated grains from meteorites imply early solar flare activity about 10^3 times that of the present Sun (Caffee et al. 1987), which might possibly correspond to similarly high mass loss rates during the first ~ 1 Gyr period of the Sun's life, but cannot be used to provide any sort of limit.

Another limit on the Sun's initial mass comes from the requirement that Mars was warm enough for liquid water to exist 3.8 Gyr ago (at the end of the late heavy bombardment period). According to Kasting (1991) and Kasting et al. (1993), this requires a solar flux (at Mars) 3.8 Gyr ago at least 13% larger than that from the standard solar model, in order to make it possible for a CO_2 greenhouse effect on Mars to be able raise the temperature to 0° C. Such an increase in flux would correspond to a mass of the Sun at that time of $M(-3.8\,\mathrm{Gyr}) \gtrsim 1.018\ M_\odot$. Since the lunar rock measurements constrain the Sun's mass ~ 3 Gyr ago to be $M(-3\,\mathrm{Gyr}) \sim 1.001\ M_\odot$, the Sun's average mass loss rate between 3.8 and 3 Gyr ago would be $\dot{M} \gtrsim 2 \times 10^{-11}\ M_\odot$/yr. If this same mass loss rate also occurred throughout the period from the Sun's birth ~ 4.6 Gyr ago until 3.8 Gyr ago, this would imply an initial solar mass of $M_i \gtrsim 1.033\ M_\odot$. Note that this lower limit assumes that the only greenhouse effect on early Mars is due to CO_2. If a smog-shielded ammonia greenhouse could exist on early Mars, such as that proposed for the early Earth by Sagan & Chyba (1997), then this lower limit on M_i might be softened or eliminated.

1.1.1. The Swenson-Faulkner Hyades Mass Loss Constraint

The earlier work of Swenson & Faulkner (1992) established that, for stars in the Hyades cluster, mass loss could not be the *major* cause of the main-sequence lithium depletion. Their result has frequently been mis-quoted and misunderstood; it has often been used to rule out the possibility of mass loss during the Sun's early main sequence phase. However, the Swenson-Faulkner results do *not* rule out relatively small amounts of mass loss for either

the Hyades or the Sun.

For the Hyades cluster, which is 0.6 Gyr old, lithium abundances in many stars have been observed, exhibiting a fairly tight relationship between a star's lithium abundance and its surface temperature — the observed lithium abundance drops off steeply with decreasing surface temperature, below $\sim$ 6000 K. Swenson & Faulkner (1992) considered lithium depletion due both to pre-main-sequence burning and to main sequence mass loss. They found that the observed lithium-temperature relationship could not be accounted for by pre-main-sequence lithium depletion alone, but that it could be accounted for fairly well if one added main sequence mass loss. However, they found that all the stars with surface temperatures below 5500 K would then have to have nearly identical initial masses (with a wide range of mass loss rates). Such a distribution of initial stellar masses, with a high, narrow peak in the distribution near 1.1 $M_\odot$, is unrealistic. This argument has been widely misquoted, to rule out early main sequence mass loss in stars (including the Sun).

The Swenson-Faulkner conclusion applies *only* if one is trying to match the Hyades lithium depletions *without including rotation-induced mixing.* As soon as one includes the latter as a major component, one can reproduce the observed lithium-temperature relation of Hyades stars by choosing suitable values for the adjustable parameters in the rotational mixing formalism (see, e.g., Charbonnel, Vauclair, & Zahn 1992). Stellar rotation is ubiquitous in young stars, and is commonly assumed to be the cause of all main sequence lithium depletion; the presence of a relatively small amount of mass loss merely requires that the large lithium depletion due to rotation be decreased by a small amount, by small changes in the adjustable parameters for rotational mixing. For the Hyades, even a mass loss as large as $\Delta M = 0.07\ M_\odot$ in a star near 1 $M_\odot$ would imply a lithium depletion factor due to mass loss alone of only $\sim$ 5, (according to the models of Swenson & Faulkner 1992), and would still require a depletion factor due to rotational mixing of $\sim$ 15 in order to reproduce the observed lithium-temperature relation. For the Sun, a mass loss of $\Delta M = 0.07\ M_\odot$ would imply lithium depletion from a combination of pre-main sequence burning and mass loss by a factor of $\sim 20 - 40$, much smaller than the total observed lithium depletion of 160 ± 40 (Grevesse & Sauval 1998); rotation would be responsible for most of the remaining lithium depletion. Mass loss of this order or less *is consistent* with the Hyades lithium observations, i.e., does not require an unrealistic initial stellar mass distribution.

In their later work, Swenson et al. (1994) found they were able to reproduce the Hyades lithium-temperature relation by pre-main-sequence depletion alone, provided that the oxygen abundance was assumed to be at the upper limit of the observed range (and using the most up-to-date OPAL and Alexander opacities). However, other clusters such as NGC 752, M67, or NGC 188 *cannot* be explained via pre-main-sequence lithium depletion alone — their

observed lithium depletions are much larger than those of the Hyades (see, e.g., Hobbs & Pilachowski 1988; Balachandran 1995), while their pre-main-sequence depletions would be significantly smaller (due to their lower metallicities). The same is true of the Sun. In other words, the observed lithium depletions demand main sequence depletion.

2. Methods

2.1. Mass Loss of the Young Sun

We computed mass-losing solar models having initial masses $M_i = 1.01$, 1.02, 1.03, 1.04, 1.05, 1.06, and 1.07 $M_\odot$; as discussed in § 1, an initial mass of 1.07 $M_\odot$ is the upper limit consistent with the requirement that the young Earth not lose its water via a moist greenhouse effect (Kasting 1988). We considered three different forms for early solar mass loss, which we call "exponential," "step-function," and "linear"; for each of these, two limiting cases are displayed in Figure 1 (i.e., cases with initial solar masses of 1.01 and 1.07 $M_\odot$).

In the "exponential" mass loss case, the mass loss rate starts out high and declines exponentially, with an initial mass loss rate $\dot{M}_0$ and decay time constant τ chosen such as to give the present observed solar mass loss rate of $\dot{M} = 3 \times 10^{-14}\ M_\odot\,\mathrm{yr}^{-1}$ at the Sun's present age. In other words, $\dot{M}(t) = \dot{M}_i\, e^{-t/\tau}$, with $\dot{M}_i = 1.33 \times 10^{-11}$ to $1.27 \times 10^{-10}\ M_\odot\,\mathrm{yr}^{-1}$ and $\tau = 0.755$ to 0.551 Gyr, for initial solar masses of 1.01 to 1.07 $M_\odot$, respectively. This exponential mass loss case is our most conservative one: a simple mass loss scenario that is still reasonably consistent with the observed lunar mass loss constraint. This scenario yields average mass loss rates over the past 3 Gyr of 13 to 42 times the present value, for initial solar masses of 1.01 to 1.07 $M_\odot$, respectively. These average mass loss values are reasonably consistent with measurements of noble gases in lunar rocks, which suggest a mass loss rate an order-of-magnitude higher than the present value. Since Figure 1 is a log-linear plot, these "exponential" mass loss cases appear as straight lines.

The "step-function" mass loss rate was chosen to have a constant high value during the period before the lunar rock observations apply, namely, the first 1.6 Gyr of the Sun's life; over the remaining 3 Gyr of the Sun's life (up to the present), a mass loss rate averaging ten times the present value was assumed, declining linearly over this period to reach the present solar mass loss rate at the present solar age. This is the most extreme case which is still consistent with the observed lunar rock mass loss constraints: it keeps the solar flux as high as possible for as long as possible. For the first 1.6 Gyr, this scenario has constant mass loss rates of $\dot{M} = 5.69 \times 10^{-12}$ to $4.32 \times 10^{-11}\ M_\odot\,\mathrm{yr}^{-1}$, for initial solar masses of 1.01 to 1.07 $M_\odot$, respectively.

In the "linear" mass loss case, the mass loss rate starts out high and declines slowly and linearly, to reach the present solar mass loss rate at the present solar age. This was chosen as our most radical case, with maximum impact on the Sun's internal structure. Due to the linear decline, the mass loss rate remains high throughout most of the Sun's lifetime, remaining of the same order as the initial mass loss rate ($\dot{M}_i = 4.35 \times 10^{-12}$ to $3.04 \times 10^{-11}\ M_\odot\,\mathrm{yr}^{-1}$, for initial solar masses of 1.01 to 1.07 $M_\odot$, respectively). During the past 3 Gyr, the mass loss rate for this "linear" case is much higher than for the other mass loss cases above, violating the observed lunar mass loss constraints (the "linear" case has average mass loss rates over the past 3 Gyr of 50 to 330 times the present rate, for initial solar masses of 1.01 to 1.07 $M_\odot$, respectively). The "linear" mass loss cases appear as curved lines in Figure 1.

2.2. Physical Inputs to our Solar Models

The solar evolution program is discussed in detail in our companion paper "Our Sun IV" (Boothroyd & Sackmann 2001); we provide only a brief summary here. We used the OPAL equation of state (Rogers, Swenson, & Iglesias 1996), extended to lower temperatures by the MHD equation of state (Däppen et al. 1988). The 1995 OPAL opacities (Iglesias & Rogers 1996) were used for $\log T > 4$; since these opacities (as well as both sets of equation of state tables) were based on the heavy element composition of Grevesse & Noels (1993), this mixture was used in order to obtain self-consistent solar models (along with their recommended value $Z/X = 0.0245$ in the present solar envelope). At lower temperatures ($\log T < 4$), the Alexander & Ferguson (1994) molecular opacities were used. Both the equation of state and the opacities were interpolated in metallicity as well as in hydrogen abundance, temperature, and density, in order to take into account metallicity variations due to diffusion and nuclear burning.

We used the NACRE nuclear reaction rate compilation (Angulo et al. 1999), supplemented by the ^{7}Be electron capture rates of Gruzinov & Bahcall (1997). Weak screening (Salpeter 1955) was used — note that it is a very good approximation to the exact quantum mechanical solution for solar conditions (see, e.g., Bahcall, Chen, & Kamionkowski 1998b; Gruzinov & Bahcall 1998). All of the stable isotopes up to and including ^{18}O were considered in detail, except for deuterium (which was assumed to have been burned to ^{3}He). The other isotopes up to ^{28}Si were included in the code, but not in the nuclear reaction network, since there are no significant effects under solar conditions (except for ^{19}F, which was assumed to be in CNO-cycle nuclear equilibrium for nuclear rate purposes). Neutrino capture cross sections were taken from Bahcall & Ulrich (1988), except for the ^{8}B-neutrino cross section

for capture on ^{37}Cl, where the more recent value (5% higher) of Aufderheide et al. (1994) was used.

A set of subroutines[2] were kindly provided to us (M. H. Pinsonneault 1999, private communication) that take into account the diffusion (gravitational settling) of helium and heavy elements relative to hydrogen (see also Thoul, Bahcall, & Loeb 1994; Bahcall, Pinsonneault, & Wasserburg 1995).

A present solar mass of $M_\odot = 1.9891 \times 10^{33}$ g (Cohen & Taylor 1986) was used, and a solar radius at the photosphere ($\tau = 2/3$) of $R_\odot = 695.98$ Mm (Ulrich & Rhodes 1983; Guenther et al. 1992). Our solar luminosity value of $L_\odot = 3.854 \times 10^{33}$ erg s^{-1} (Sackmann, Boothroyd, & Kraemer 1993) is close (less than 1-*sigma*) to the more recent value of Bahcall, Pinsonneault, & Basu (2001); as discussed in our companion "Our Sun V" paper (Boothroyd & Sackmann 2001), such a luminosity difference has negligible effect on the solar structure (and only a minor effect on the neutrino rates). We used a solar age of $t_\odot = 4.6$ Gyr, measured from the Sun's birth on the pre-main-sequence Hayashi track; this is close to the range 4.55 Gyr $< t_\odot <$ 4.59 Gyr allowed by meteoritic ages Bahcall et al. (1995). Our models took about 40 Myr to reach the zero age main sequence (ZAMS), the point at which nuclear reactions in the core provide essentially all the Sun's luminosity, and the pre-main-sequence contraction stops; this pre-main-sequence timescale implies that the *total solar age* $t_\odot$ used in this paper can be converted into a *main sequence* solar lifetime by subtracting about 0.04 Gyr.

We investigated the effects of using two different zonings. Our coarse-zoned models had about 2000 spatial zones in the model, and about 200 time steps in the evolution from the zero-age main sequence to the present solar age (plus about 800 time steps on the pre–main-sequence). Typically, these models were converged to match the solar luminosity, radius, and surface Z/X value to within a few parts in 10^5; a few cases where convergence was slow reached only about a part in 10^4. Our fine-zoned models had 10 000 spatial zones and took 1500 main-sequence time steps (plus 6000 pre–main-sequence time steps) — a factor of 5 increase in both spatial and temporal precision — but because of the much larger amounts of CPU-time required, they were converged to match the solar luminosity, radius, and surface Z/X value with no better accuracy than the coarse-zoned cases. The standard solar models were converged to an accuracy nearly a factor of ten better than the typical mass-losing models. As dicussed in our companion "Our Sun V" paper (Boothroyd & Sackmann 2001), even the worst of the above convergence accuracies has a negligible effect on the solar sound speed profile: up to 1 or 2 parts in 10^4 in the convective envelope, and a

[2]These subroutines are available from Bahcall's web page: http://www.sns.ias.edu/~jnb/

few parts in 10^5 below it.

We compared our solar models to profiles of the solar sound speed $c_\odot$, density $\rho_\odot$, and adiabatic index $(\Gamma_1)_\odot$ obtained from the helioseismic reference model of Basu et al. (2000)[3], which they obtained by inversion from the helioseismic frequency observations. In the inversion process, a standard solar model is required, but Basu et al. (2000) demonstrated that the resulting $c_\odot$ and $\rho_\odot$ profiles of the helioseismic reference model are relatively insensitive to uncertainties in the standard solar model used for this purpose (except for uncertainties in $R_\odot$). They estimated a net uncertainty of few parts in 10^4 for the sound speed $c_\odot$ and adiabatic index $(\Gamma_1)_\odot$, and a few parts in 10^3 for the density $\rho_\odot$. However, in the Sun's core ($r \lesssim 0.1\ R_\odot$), systematic uncertainties in the helioseismic sound profile are increased by a factor of ~ 5; this was demonstrated by Bahcall et al. (2001), who compared helioseismic inversions of different helioseismic data sets. We used their comparison to estimate the r-dependence of the systematic error in $c_\odot$ in the core and in the convective envelope (namely, a fractional systematic error decreasing linearly from 0.0013 at $r = 0.05\ R_\odot$ to 0.0003 at $r = 0.2\ R_\odot$, constant from there to $r = 0.72; R_\odot$, then increasing linearly to 0.00052 at $r = 0.94; R_\odot$). For $c_\odot$, this systematic error can be significantly larger than the statistical errors, and we combined the two in quadrature to get the fractional error (σ_c/c) for the purpose of calculating weighted rms differences — the rms fractional difference in c is given by $\left(\left\{\sum[(\Delta c/c)/(\sigma_c/c)]^2\right\} / \left\{\sum[1/(\sigma_c/c)]^2\right\}\right)^{1/2}$. For $(\Gamma_1)_\odot$ and $\rho_\odot$, the systematic errors are comparable to or smaller than the statistical ones, and the statistical errors sufficed for calculating weighted rms differences.

We present all our sound speed and density profiles in terms of differences relative to the observed helioseismic reference profiles. This choice of presentation not only allows one to see the effects of the choice of initial mass and mass loss type, but also the extent to which the models agree with the helioseismic observations.

3. Results and Discussion

For comparison with our solar mass loss rates, we used the most recent observed upper limits on stellar mass loss rates from three young Sun-like stars (namely, $\dot{M} \lesssim 5 \times 10^{-11}\ M_\odot\,\mathrm{yr}^{-1}$, from π^{01} UMa, κ^1 Cet, and β Com), as presented by Gaidos et al. (2000). Even our highest mass loss cases are close to being consistent with these limits, as is illustrated in Figure 1.

[3]From the denser-grid machine-readable form of their Table 2, at http://www.sns.ias.edu/~jnb/

3.1. Testing Mass Loss Models Via Helioseismology

3.1.1. Sound Speed and Density Profiles

We present in Figure 2 profiles of the adiabatic sound speed differences $\delta c/c \equiv (c_\odot - c_{model})/c_\odot$; profiles of the density differences $\delta\rho/\rho \equiv (\rho_\odot - \rho_{model})/\rho_\odot$ are available online[4]. Solar masses as a function of time for the corresponding cases are presented in Figure 3, and solar fluxes at the planets (relative to their present values) are presented in Figure 4.

Since the prominent peak at $r \sim 0.7\ R_\odot$ results from the neglect of rotational mixing, we did not require agreement in this region between profiles from our theoretical models and profiles inferred from the helioseismic observations. Nor did we require agreement in core region, since the present helioseismic observations still result in large uncertainties in the inferred profiles there. On the other hand, we aimed for agreement in the regions $0.1\ R_\odot \lesssim r \lesssim 0.6\ R_\odot$ and $0.72\ R_\odot \lesssim r \lesssim 0.94\ R_\odot$, where disagreements are due to imperfections in the input physics or uncertainties in the observed solar parameters. This is demonstrated by our variant models of our companion paper "Our Sun IV" (Boothroyd & Sackmann 2001) and of Morel et al. (1997) and Basu et al. (2000).

Figure 2a demonstrates that all of our "exponential" mass loss models agree better with the helioseismic observations than the standard solar model without mass loss (i.e., they lie closer to the zero line of perfect agreement). The rms sound speed differences provide a numerical measure of the extent of the above agreement between a given theoretical model and the profile inferred from helioseismic observations; these rms values for each of our mass-losing cases are given in Table 1. When one considers the whole of the Sun (from center to surface), the rms sound speed difference is 0.0013 for the standard solar model, while the corresponding rms is 0.0010 for our most extreme "exponential" mass loss case (with $M_i = 1.07\ M_\odot$) — this extreme "exponential" mass loss case agrees 25% better with the helioseismic observations than the standard solar model. As discussed in the previous paragraph, the prominent peak near $0.7\ R_\odot$ results from the neglect of rotation; if one considers the rms difference for the region deeper inside the Sun (i.e., $r < 0.6\ R_\odot$), the rms is 0.0009 for the standard solar model, while the rms is 0.0006 for our most extreme "exponential" mass loss case ($M_i = 1.07\ M_\odot$) — a similar improvement. However, these improvements are not statistically significant, as discussed in the next paragraph.

As pointed out by our companion paper "Our Sun IV" (Boothroyd & Sackmann 2001), there are non-negligible uncertainties in any theoretical solar model, due to uncertainties

[4]http://www.krl.caltech.edu/~aib/papdat.html

in Z/X, opacity, nuclear reaction rates, solar age, solar radius, rotation, diffusion rates, and equation of state. When these physical effects are varied within their likely uncertainty range, they give rise to variations in the sound speed profiles of theoretical solar models. The rms differences (over the entire Sun) of these variant solar models relative to the reference standard solar model are typically of the order of 0.0010, and in extreme cases can be double this amount (see Table 2 of our companion paper "Our Sun IV": Boothroyd & Sackmann 2001). The variations caused by our "exponential" mass loss are considerably less than the variations caused by the uncertainties in the other physical quantities mentioned above. Even our most extreme "exponential" case ($M_i = 1.07\ M_\odot$) differs from the standard solar model by an rms of only 0.0006 in the sound speed, as compared to the rms uncertainty of up to 0.0020 from other causes.

In other words, none of our "exponential" mass loss cases with initial solar masses $M_i \lesssim 1.07\ M_\odot$ can be ruled out by helioseismological observations; in fact, all other things being equal, these helioseismological observations mildly favor the "exponential" mass loss case with highest of our initial solar masses ($M_i = 1.07\ M_\odot$), as shown by Figure 2a and the rms values in Table 1.

Figure 2b presents our results for our "step-function" mass loss models; recall that this type of mass loss was chosen as the most extreme possibility that remains consistent with the observational mass loss constraints (see § 2.1). Since the Sun remains more massive for a longer period in this case than for the "exponential" mass loss cases (compare Fig. 3b with Fig. 3a), there is more of an impact on the Sun's internal structure (compare Fig. 2b with Fig. 2a). Again, the mass-losing models all fit better than the standard (non-mass-losing) model, as shown by Figure 2b and the rms values in Table 1. The $M_i = 1.05$ and $1.06\ M_\odot$ cases fit best, having the lowest rms error (of 0.0006 for $r < 0.6\ R_\odot$) relative to the sound speed profile inferred from helioseismic observations (cf. 0.0009 for the standard model). As before, the variations caused by our mass loss are considerably less than the variations caused by the uncertainties in the other physical quantities. Even our most extreme "step-function" case ($M_i = 1.07\ M_\odot$) differs from the standard solar model by an rms of only 0.0010 in the sound speed, as compared to the rms uncertainty of up to 0.0020 from other causes. As in the "exponential" mass loss case, none of the "step-function" mass loss cases can be ruled out by helioseismic observations.

Figure 2c presents our results for the radical "linear" mass loss models; recall that these models violate the solar wind constraints from the lunar rock observations by about an order of magnitude (see § 2.1). Since the Sun remains remains more massive for a very long time compared to the other mass loss cases (compare Fig. 3c with Fig. 3a, b), there is even more of an impact on the Sun's internal structure (compare Fig. 2c with Fig. 2a, b). Only the

lower initial masses (namely, $M_i \lesssim 1.05\ M_\odot$) fit better than the standard (non-mass-losing) model, as shown by Figure 2c and the rms values in Table 1. The masses $M_i = 1.01$ through $1.04\ M_\odot$ cases fit best, having the lowest rms error (of 0.0007 for $r < 0.6\ R_\odot$) relative to the sound speed profile inferred from helioseismic observations (cf. 0.0009 for the standard model). The variations caused by our mass loss remain somewhat less than the variations caused by the uncertainties in the other physical quantities. Even our most extreme "linear" case ($M_i = 1.07\ M_\odot$) differs from the standard solar model by an rms of only 0.0016 in the sound speed, as compared to the rms uncertainty of up to 0.0020 from other causes. Even these radical "linear" mass loss cases cannot be ruled out by comparisons with the helioseismic observations.

3.1.2. Position of Convection and Surface Helium Abundance

Helioseismic observations measure the position of the base of the Sun's convective envelope, namely $R_{ce} = 0.713 \pm 0.001\ R_\odot$ (Basu & Antia 1997), and the surface helium abundance, namely, a mass fraction Y_e in the range $0.24 \lesssim Y_e \lesssim 0.25$ (see discussion in our companion paper "Our Sun IV": Boothroyd & Sackmann 2001). The values of R_{ce} and Y_e for both our reference standard solar model and for all of our mass-losing models are shown in Table 1. The mass-losing cases all have values of R_{ce} and Y_e very close to those of the standard solar model, all of them being consistent with the helioseismic observations.

3.2. Other Effects of Modest Mass Loss

3.2.1. Solar Lithium Depletion

The lithium depletion in a main sequence star, relative to its initial lithium abundance, can result from three different causes. There can be significant lithium depletion from pre-main-sequence lithium burning at early times, when the convective envelope reaches deep into the star. Rotationally induced mixing on the main sequence can transport lithium down from the convective envelope to regions hot enough for lithium burning. Mass loss on the main sequence can cause the convective envelope to move inwards and engulf lithium-depleted regions. The Sun's initial lithium abundance is assumed to be equal to the meteoritic abundance, and the depletion factor $f_{\rm Li}$ is obtained by comparing this initial abundance with the present observed solar photospheric lithium abundance.

The observed solar lithium depletion factor is $f_{\rm Li} = 160 \pm 40$ (Grevesse & Sauval 1998). For pre-main-sequence lithium depletion, our reference standard solar model predicts a

lithium depletion factor is $f_{\rm Li} = 24$, although this is very sensitive to the solar metallicity (i.e., Z/X value, as well as uncertainties in diffusion) and to the choice of low-temperature molecular opacities; values of $f_{\rm Li}$ from 11 to 70 can be obtained (see our companion paper "Our Sun IV": Boothroyd & Sackmann 2001). For rotation-induced main sequence lithium depletion, there is no theoretical prediction; instead, the observed main sequence lithium depletion is used to constrain the free parameters in the theoretical treatment (see, e.g., Schatzman 1977; Lebreton & Maeder 1987; Pinsonneault et al. 1989; Richard et al. 1996). For main sequence mass loss, the extent of main sequence lithium depletion depends primarily on the initial solar mass, and only weakly on the timescale of mass loss. Boothroyd et al. (1991) used the observed solar lithium depletion to obtain a limit on solar main sequence mass loss, finding that the maximum mass loss allowed was 0.1 $M_\odot$ (i.e., a maximum initial solar mass of $M_i \approx 1.1\ M_\odot$). However, as discussed in § 1, such an extreme mass loss case violates the constraint from the requirement that the early Earth not lose its water via a moist greenhouse effect, which would occur for $M_i > 1.07\ M_\odot$. This constraint is based on a cloud-free climate model; a very slight increase in M_i might be allowed if clouds were taken into account.

As the Sun's initial mass is increased above 1 $M_\odot$, there are two competing effects. Higher initial masses have less pre–main-sequence lithium depletion; on the other hand, the higher the initial mass, the more mass loss has to take place, and thus the more lithium depletion takes place on the main sequence (as the convective envelope sheds lithium-rich material from the surface and ungulfs lithium-depleted material from below). As may be seen from Table 1, for initial solar masses in the range $1.01\ M_\odot \leq M_i \lesssim 1.04\ M_\odot$, the first of these effects dominates, and the total lithium depletion is slightly less than in the standard (non-mass-losing) model; slightly stronger rotation-induced mixing would be required in order to account for the observed lithium depletion. For masses $M_i \gtrsim 1.05\ M_\odot$, the mass loss dominates; however, even for our most extreme mass loss case ($M_i = 1.07\ M_\odot$), the total lithium depletion is only $f_{\rm Li} = 34$, 50, or 49 for the "exponential," "step-function," or "linear" mass loss cases, respectively. There is at most factor of 2 more lithium depletion than in the standard (non-mass-losing) model (with $f_{\rm Li} = 24$).

The modest amount of mass loss considered here ($\Delta M \leq 0.07\ M_\odot$) has only a minor effect on the extent of solar lithium depletion — smaller than the effects on pre-main-sequence lithium depletion caused by uncertainties in other physical parameters, as discussed above and in our companion paper "Our Sun IV": (Boothroyd & Sackmann 2001). In these mass-losing models, rotational mixing would still be required, to account for the majority of the Sun's observed lithium depletion. The observed solar lithium depletion thus cannot be used to constrain these mass-losing solar models.

In a previous paper (Boothroyd et al. 1991), we had obtained an upper limit on solar mass loss of $\Delta M \approx 0.11\ M_\odot$. In this limiting case, the lithium depletion would be caused only by pre-main-sequence burning and mass loss, with no effect from rotational mixing. By considering lithium depletion in the Hyades, Swenson et al. (1994) showed that this limiting case could not actually occur: mass loss could not be responsible for the majority of the Hyades lithium depletion. However, the cases $\Delta M \leq 0.07\ M_\odot$ considered in this paper, where mass loss has only a minor effect on lithium depletion, are not ruled out by their arguments.

3.2.2. Solar Beryllium Depletion

The observed solar beryllium abundance is $\log \epsilon(^9\mathrm{Be}) = 1.40 \pm 0.09$, consistent with no depletion relative to the meteoritic value of $\log \epsilon(^9\mathrm{Be}) = 1.42 \pm 0.04$. These values imply that solar beryllium cannot have been depleted by more than a factor of 2 (3-σ upper limit). A standard solar model has negligible beryllium depletion ($\sim 1\%$); our mass-losing solar models predict larger depletions, but are still all consistent with the observational limit. The most extreme of the "exponential" mass loss cases ($M_i = 1.07\ M_\odot$) depleted beryllium by a relatively small amount (a factor of 1.17). Even the most extreme of the "step-function" and "linear" mass loss cases yielded only $\sim$ 2-σ beryllium depletion factors of 1.53 and 1.63, respectively; the $M_i = 1.04\ M_\odot$ cases depleted beryllium by negligible amounts, less than 3%.

3.2.3. Neutrino Fluxes

As may be seen from Table 1, the modest mass loss considered here has almost no effect on the predicted solar neutrino fluxes. Variations are at most a few percent in the predicted ^{8}B flux and in the predicted capture rate for the chlorine experiment (as compared to uncertainties of $\sim 30\%$ from other causes), and less than a percent in the predicted capture rate for the gallium experiment (as compared to uncertainties of at least several percent from other causes) — the other sources of uncertainty in neutrino fluxes are discussed elsewhere (see, e.g., Boothroyd & Sackmann 2001; Bahcall et al. 2001, 1995).

3.3. The Young Earth and the Solar Flux

For Earth, the greenhouse effect at present raises the surface temperature by 33° C. At present, an airless, rapidly-rotating body at Earth's orbit would have a temperature

of $-18°$ C (255 K), if it had Earth's present albedo and emissivity (Sagan & Chyba 1997), but the Earth's present mean surface temperature is observed to be $+15°$ C (288 K). The difference is due to greenhouse gases in the Earth's atmosphere, primarily CO_2 and H_2O. If the atmospheric CO_2 abundance were *constant* (at its present value), and the H_2O abundance were determined by its equilibrium vapor pressure, then 2 Gyr ago the Earth's surface temperature would have been below 0° C (Sagan & Mullen 1972; Sagan 1977; Pollack 1979). If the early Earth's surface temperature were below the freezing point of water, extensive glaciation would be expected; such glaciation would raise the Earth's albedo, delaying the time when the surface temperature reached 0° C. In other words, one would expect Earth to be fully glaciated as recently as 1 Gyr in the past (North 1975; Wang & Stoner 1980)).

On the other hand, a number of independent observations indicate that the Earth was at least warm enough for liquid water to exist as far back as 4 Gyr ago. Liquid water is necessary to explain the existence of the widespread microorganisms whose fossils are found in rocks dated as far back as 3.8 Gyr ago (Cogley & Henderson-Sellers 1984; Mojzsis et al. 1996; Eiler et al. 1997). Tidal or intertidal stromatolite fossils have been dated to ~ 3.5 Gyr ago, alluvial detrital uraninite grains as far back as 3 Gyr, and turbidites and ripple marks have been dated as far back as 3.5 Gyr (Eriksson 1982). Sedimentary rocks, which are laid down under water, have been dated to at least 4 Gyr ago (Bowring et al. 1989; Nutman et al. 1984).

In fact, there is evidence not only that liquid water existed on the early Earth, but also that Earth was considerably warmer in the past than it is today. To start with, there is no evidence of glaciation before 2.7 Gyr ago (Kasting 1989), and it has been suggested that tillites prior to 2 Gyr ago are actually due to impacts rather than glaciers (Oberbeck et al. 1993). Archaeobacteria exhibit extreme thermophilic trends (Woese 1987). High ocean temperatures of $\sim 40°$ C in the period 2.6 to 3.5 Gyr ago are suggested by sulphur isotope measurements (Ohmotu & Felder 1987). Average surface temperatures of tens of degrees Celsius in the period 2.5 to 3.5 Gyr ago are indicated by deuterium to ^{18}O ratios (Knauth & Epstein 1976). Temperatures as high as 80° C in the period ~ 3.8 Gyr ago are suggested by differences in ^{18}O isotopic data between coexisting cherts and phosphates (Karhu & Epstein 1986), although the results are subject to interpretation.

The above "weak Sun paradox", of a faint young Sun and a warm young Earth, has traditionally been explained by invoking a much stronger greenhouse effect, driven by extremely high (i.e., *non-constant*) CO_2 concentrations in Earth's early atmosphere (partial CO_2 pressures of order a few bars: see, e.g., Pollack 1979; Kuhn & Kasting 1983; Kasting & Ackerman 1986). Qualitatively, high CO_2 concentrations can be justified on the basis of theoretical feedback mechanisms linking mineral dissolution to liquid water and thus to

atmospheric CO_2 (Walker, Hays, & Kasting 1981). Although such massive amounts of CO_2 in the Earth's early atmosphere are a possible solution to the "weak Sun paradox", they are not mandated; there is little experimental evidence available on which to base a choice of CO_2 concentration (Canuto et al. 1983; Kuhn, Walker, & Marshall 1989). Indeed, very high concentrations may prove to be inconsistent with derived weathering rates (Holland, Lazar, & McCaffrey 1986). The recent work of Rye et al. (1995) places an upper limit of 0.04 bar on the partial pressure of CO_2 in the period from 2.75 to 2.2 Gyr ago, based on the absence of siderite in paleosols. Actual measurements of CO_2 abundances are available only for relatively recent times, i.e., only for the last $\sim$ 0.45 Gyr (see, e.g., Crowley & Berner 2001; Retallack 2001). These latter measurements show major variations in the CO_2 abundance over the past 0.45 Gyr. The lowest values are comparable to the present-day CO_2 abundance of about 350 ppmV (or the pre-industrial-age value of $\sim$ 300 ppmV); the highest value measured over the last 0.45 Gyr are $\sim$ 5000 ppmV. However, from these measurements, there is no clear evidence of a long-term trend of higher CO_2 abundances in the relatively recent past (i.e., the last 0.4 Gyr).

A non-CO_2 greenhouse has been suggested for the early Earth (Kasting 1982; Lovelock 1988). Recently, Sagan & Chyba (1997) calculated that a strong greenhouse contribution from ammonia was possible, if a concentration of $[NH_3] \sim 10^{-5}$ could be maintained. Normally, the ammonia would be photodissociated by solar UV flux on a timescale of 10 years. They pointed out that ammonia could be shielded from the UV radiation by high-altitude organic solids produced from photolysis of methane — a photochemical smog, similar to that observed in the upper atmosphere of Titan (Ragas & Pollack 1980). However, the ammonia lifetime depends sensitively on two parameters, the fraction f of the methane irradiation products that are organic solids, and the sedimentation timescale t of the smog; Sagan & Chyba (1997) take as reasonable values $f \gtrsim 0.1$ and 0.5 yr $\lesssim t \lesssim$ 3 yr. For $f \gtrsim 0.5$, or $t \sim 3$ yr, the ammonia lifetime is long enough for the required ammonia concentration to be maintained, given a reasonable amount of resupply. However, for $f \sim 1$ and $t \lesssim 1$ yr, the ammonia lifetime is less than 200 yr, which would require excessively large amounts of ammonia production to maintain the required ammonia greenhouse effect. Sagan & Chyba (1997) also note that an atmosphere rich in N_2, with minor CO_2 and CH_4 components, could have adequate self-shielding of NH_3 from photodissociation (allowing an ammonia greenhouse), only as long as the ratio $CH_4/CO_2 \gtrsim 1$ was maintained. In other words, for the early Earth, a smog-shielded ammonia greenhouse is a viable solution to the "weak Sun paradox" under certain conditions, but fails under others.

As discussed above, it is not clear whether the greenhouse effect could suffice to warm the early Earth. A bright young Sun, with stronger illumination of the young Earth than from the standard solar model, would require a less extreme early greenhouse effect to prevent

the early Earth from freezing over.

3.4. The Young Mars and the Solar Flux

For Mars, there are also indications of higher surface temperatures in the past, that are even harder to explain by a greenhouse effect. There is evidence of large scale flow of liquid water ~ 3.8 Gyr ago, from the drainage channels and valley networks visible on the heavily cratered ancient surface of Mars (Pollack et al. 1987; Carr 1996); there is some evidence for lakes (Goldspiel & Squyres 1991; Parker et al. 1993), and possibly even oceans 3 to 4 Gyr ago (Schaefer 1990; Baker et al. 1991). Even if the channels were formed by subsurface sapping of groundwater, Martian surface temperatures significantly higher than today would have been required for liquid water to be present near the surface; if the suggested evidence of glacial markings were confirmed, this would require temperatures high enough for precipitation to occur (Whitmire et al. 1995).

Kasting (1991) demonstrated that there is an upper limit to the greenhouse warming of Mars that is possible from CO_2. He showed that the maximum possible greenhouse warming occurs at a Martian surface CO_2 pressure of 5 bars — with more CO_2, the added greenhouse warming is outweighed by the cooling effects of increased CO_2 condensation in the upper Martian atmosphere. He demonstrated that the requirement of liquid water on Mars, i.e., a surface temperature of at least 273° K, demands a solar flux value $S \geq 0.86$ (where S is the solar flux relative to its present value), even with the most favorable greenhouse warming case of a CO_2 pressure of 5 bars. At 3.8 Gyr ago, when liquid water is thought to have existed on Mars, the standard solar model yields a value of $S = 0.75$ (see Fig. 4), totally insufficient relative to Kasting's minimum value of 0.86. Kasting (1991) states that the uncertainties in his Martian climate model might push the limiting value of S from 0.86 down to 0.80 (albeit for an unreasonably low Martian albedo), but even this lower S requirement is incompatible with the standard solar model. The standard solar model does not reach this extreme limit of $S = 0.80$ until 2.9 Gyr ago, and reaches $S = 0.86$ later still, at 1.9 Gyr ago (see Fig. 4) — in either case, far too late to account for liquid water on Mars 3.8 Gyr ago. With CO_2 pressures either lower or higher than 5 bar, Kasting (1991) shows that even higher solar flux values would be required to yield liquid water. He presents the solar flux required to obtain liquid water as a function of the CO_2 pressure: e.g., a pressure of 3 bar would require $S \gtrsim 0.92$, and a pressure of 10 bar would require $S \gtrsim 0.90$. The standard solar model is totally incapable of yielding such high fluxes 3.8 Gyr ago (see Fig. 4). In other words, for a standard solar model, CO_2 greenhouse warming cannot under any circumstances yield liquid water on early Mars.

Yung, Nair, & Gerstell (1997) have suggested that small amounts of SO_2 might have served as a powerful source of heating in the upper atmosphere of early Mars (due to its strong absorption in the near UV), which might have been sufficient to prevent the condensation of CO_2. However, in their preliminary investigation, they did not investigate the photochemistry of SO_2 — it has a very short photochemical lifetime, and also produces H_2SO_4, which leads to cooling.

Some temperature increase on early Mars is expected from geothermal heating (Squyres 1993), but by itself it is insufficient (Whitmire et al. 1995).

With the above greenhouse and geothermal heating apparently incapable of yielding liquid water on early Mars, given the illumination from a standard solar model, let us consider the possibility of a non-standard, brighter young Sun. Figure 4 presents the relative flux values S throughout the Sun's past history yielded by our mass-losing solar models with initial masses from $M_i = 1.01$ to $1.07\ M_\odot$ (as well as that from a standard solar model). The requirement that the early Earth not lose its water via a moist greenhouse effect leads to an upper limit of $S \leq 1.1$, corresponding to the upper edge of the figures. The lower luminosity constraints from the requirement that liquid water be present 3.8 Gyr ago on early Mars are shown by the vertical arrows; the heavy double arrow corresponds to the limit $S \geq 0.86$ obtained by Kasting (1991), and the lighter single arrow to his extreme (less probable) limit $S \geq 0.80$.

Figure 4a presents the solar flux S at Earth and Mars (relative to their present flux) from the time of solar system formation until the present, for our "exponential" mass loss cases; the flux for the standard solar model (without mass loss) is also shown, by the solid line. Note that the mass loss time scale is between 0.755 and 0.551 Gyr, with initial mass loss rates from 1.33×10^{-11} to $1.27 \times 10^{-10}\ M_\odot\ \mathrm{yr}^{-1}$, for initial masses from 1.01 to $1.07\ M_\odot$, respectively. The exponential decline as a function of time of these mass loss rates means that they are generally consistent with the observations of π^{01} UMa, κ^1 Cet, and β Com presented by Gaidos et al. (2000), who obtained upper limits of 5×10^{-11}, 4×10^{-11}, and $4 \times 10^{-11}\ M_\odot\ \mathrm{yr}^{-1}$, respectively, for the mass loss rates of these three young Sun-like stars (note that the $M_i = 1.07\ M_\odot$ case is only marginally consistent, lying very slightly above the π^{01} UMa limit: see Fig. 1). Our results demonstrate that, for the "exponential" mass loss cases, the $M_i = 1.07\ M_\odot$ case — and only this case — is marginally consistent with the Kasting (1991) Mars flux requirement $S \gtrsim 0.86$ at an age of ~ 3.8 Gyr ago; if the Martian surface CO_2 pressure 3.8 Gyr ago was either much lower or much higher than 5 bar, even the $M_i = 1.07\ M_\odot$ case would be ruled out. (If the unlikely extreme Kasting flux limit of $S \gtrsim 0.80$ is used, initial masses $1.03\ M_\odot \lesssim M_i \lesssim 1.07\ M_\odot$ would be permissible for a CO_2 pressure of 5 bars, and the $M_i = 1.07\ M_\odot$ case would be marginally compatible with pressures

between ~ 3 and ~ 12 bar.) It is interesting that the $M_i = 1.07\ M_\odot$ case, which is favored by the observations of water on early Mars, is also mildly favored the helioseismic frequency observations (see § 3.1), and is in reasonable agreement with the lunar rock observations of the solar wind over the past 3 Gyr.

Figure 4b similarly presents the extreme "step-function" mass loss case. This case has a constant mass loss rate for the first 1.6 Gyr ($\dot{M} = 5.69 \times 10^{-12}$ to $4.32 \times 10^{-11}\ M_\odot\,\mathrm{yr}^{-1}$, for initial solar masses of 1.01 to 1.07 $M_\odot$, respectively), and a low mass loss rate thereafter. These mass loss rates are all consistent with the stellar mass loss observations of Gaidos et al. (2000) for π^{01} UMa, κ^1 Cet, and β Com quoted above. These "step-function" cases have a longer mass loss timescale than the "exponential" one, and thus yield a higher solar flux for the first 1.6 Gyr. (Due to the way the "step-function" cases were defined, after the first 1.6 Gyr their solar flux is very close to that of the standard solar model.) Our results demonstrate that, for this extreme "step-function" mass loss case, initial masses $1.04\ M_\odot \lesssim M_i \lesssim 1.07\ M_\odot$ are capable of yielding liquid water on Mars until 3.8 Gyr ago. Again, these higher mass cases, which are favored by the observations of water on early Mars, are also mildly favored by the helioseismic frequency observations (see § 3.1); these "step-function" mass loss cases were defined in such a way as to be in agreement with the lunar rock observations of the solar wind over the past 3 Gyr.

Figure 4c similarly presents the radical "linear" mass loss case. This case has a high initial mass loss rate ($\dot{M} = 4.35 \times 10^{-12}$ to $3.04 \times 10^{-11}\ M_\odot\,\mathrm{yr}^{-1}$, for initial solar masses of 1.01 to 1.07 $M_\odot$, respectively), which remains relatively high throughout much of the Sun's lifetime (since it declines linearly with time to reach the present solar mass loss rate at the present time). These mass loss cases are consistent with the stellar mass loss observations of Gaidos et al. (2000) for π^{01} UMa, κ^1 Cet, and β Com quoted above. However, they are *not* consistent with the lunar rock observations of the solar wind over the past 3 Gyr, violating this latter constraint by an order of magnitude. Our results demonstrate that, for this radical "linear" mass loss case, initial masses $1.03\ M_\odot \lesssim M_i \lesssim 1.07\ M_\odot$ are capable of yielding liquid water on Mars until 3.8 Gyr ago; the lower end of this range is mildly favored by the helioseismology. Note that these preferred cases $M_i = 1.03$ and $1.04\ M_\odot$ have remarkably constant solar flux over the first 3 Gyr.

3.5. The Favored Cases of a Bright Young Sun

A mass-losing solar model will always be brighter at birth than the standard solar model, since the luminosity L_{ZAMS} at the zero age main sequence (ZAMS) is roughly proportional to the mass to the fourth power ($L_{ZAMS} \propto M_i^4$). For a mass-losing Sun, the orbital radii of

the planets varies inversely with the solar mass ($r_i \propto 1/M_i$, due to conservation of angular momentum); the initial flux at the planets is thus proportional to the sixth power of the initial solar mass ($F_{ZAMS} \propto L_{ZAMS}/r_i^2 \propto M_i^6$). Figure 4 illustrates the solar flux at the planets as a function of time, demonstrating how much higher the early solar flux at the planets is in the mass-losing cases than in the standard (non-mass-losing) model.

For clarity, only the flux for our preferred initial masses for each type of mass loss are illustrated in Figure 5. Our preferred "exponential" case predicts a solar flux at the planets about 5% higher at birth than at present, considerably higher than that indicated by the standard solar model (which predicts a flux 29% lower than at present). At 3.8 Gyr ago, the flux for our "exponential" case would have been only 16% lower than at present (cf. 25% for the standard model). For our preferred "step-function" case, the flux at the planets would have been only 10% lower at birth than at present (cf. 29% for the standard model); at 3.8 Gyr ago, the flux would have been only 14% lower than at present (cf. 25% for the standard model). For these "exponential" and "step-function" cases, the flux at the planets for the past 3 billion years would be essentially the same as that predicted by the standard solar model. Our radical "linear" case would have had an almost constant solar flux at the planets for the first 3 Gyr, namely, only 11% lower than at present (cf. 29% to 12% lower for the standard model); for this case, the flux would be close to that predicted by the standard solar model only during the last billion years.

Figure 6 presents the evolution in the HR diagram of our preferred mass-losing cases (heavy dashed and dot-dashed curves); these cases are in agreement with helioseismic observations, with the existence of water on early Mars, and with lunar rock observations of solar mass loss. (A radical case, agreeing with the first two of these constraints but disagreeing with the third one, is shown by the light dotted curve.) For comparison, the standard solar model is also displayed (solid line). Figure 6 illustrates that the early evolution of mass-losing solar models is in the opposite direction in the HR diagram to the standard solar model: the mass-losing models initially become less luminous and slightly redder (instead of more luminous and slightly bluer). Figure 6 also illustrates that in the past, the Sun's surface temperature changed only by negligible amounts (1 or 2%), both for the standard and the mass losing cases, in contrast to the relatively large changes in the luminosity.

4. Conclusions

A slightly higher initial solar mass, producing a brighter young Sun, turns out to be a viable explanation for warm temperatures on early Earth and Mars. Such a higher initial solar mass leaves a fingerprint on the Sun's present internal structure that is large enough

to be detectable via helioseismic observations. Our computations demonstrated that all 21 of the mass-losing solar models that we considered were consistent with the helioseismic observations; in fact, our preferred mass-losing cases were in marginally better agreement with the helioseismology than the standard solar model was. However, there are still significant uncertainties in the observed solar composition and in the input physics on which the solar models are based; these uncertainties have a slightly larger effect on the Sun's present internal structure than the fingerprint left from early solar mass loss. Future improvements in the accuracy of these input parameters could reduce the size of the uncertainties below the level of the fingerprints left by a more massive, brighter young Sun, allowing one to determine whether early solar mass loss took place or not. Also urgently needed are more measurements of mass loss rates from other young stars similar to the young Sun, and more measurements from our solar system that can be used to estimate the solar wind in the past.

We wish to thank Prof. Charles A. Barnes and Prof. Yuk L. Yung for thoughtful discussions and encouragement. We are grateful to Prof. Robert D. McKeown for the support provided by the W. K. Kellogg Radiation Laboratory. One of us (I.-J. S.) wishes to thank Alexandra R. Christy, her daughter, and Prof. Robert F. Christy, her husband, for their supportiveness, and Robert F. Christy for critical analysis and helpful comments. One of us (A. I. B.) wishes to thank Prof. Peter G. Martin and Prof. J. Richard Bond for their support, and M. Elaine Boothroyd, his wife, for her patience and encouragement. This work was supported by a grant NAG5-7166 from the Sun-Earth Connection Program of the Supporting Research and Technology and Suborbital Program in Solar Physics of the National Aeronautics and Space Administration, and by the National Science Foundation grant NSF-0071856 to the Kellogg Radiation Laboratory.

REFERENCES

Alexander, D. R., & Ferguson, J. W. 1994, ApJ, 437, 879

Angulo, C. et al. 1999, Nucl. Phys. A, 656, 3

Aufderheide, M. B., Bloom, S. B., Resler, D. A., & Goodman, C. D. 1994, Phys. Rev. C, 49, 678

Baker, V. R., Strom, R. G., Gulick, V. C., Kargel, J. S., Komatsu, G., & Kale, V. S. 1991, Nature, 352, 589

Bahcall, J. N., Chen, X. L., & Kamionkowski, M. 1998, Phys. Rev. C, 57, 2756

Bahcall, J. N., Pinsonneault, M. H., & Basu, S. 2001, ApJ, 555, 990

Bahcall, J. N., Pinsonneault, M. H., & Wasserburg, G. J. 1995, Rev. Mod. Phys., 67, 781

Bahcall, J. N., & Ulrich, R. K. 1988, Rev. Mod. Phys., 60, 297

Balachandran, S. 1995, ApJ, 446, 203

Basu, S., & Antia H. M. 1997, MNRAS, 287, 189

Basu, S., Pinsonneault, M. H., & Bahcall, J. N. 2000, ApJ, 529, 1084

Boothroyd, A. I., & Sackmann, I.-J. 2001, ApJ, submitted

Boothroyd, A. I., Sackmann, I.-J., & Fowler, W. A. 1991, ApJ, 377, 318

Bowring, S. A., Williams, I. S., & Compston, W. 1989, Geology, 17, 971

Brown, A., Vealé, A., Judge, P., Bookbinder, J. A., & Hubeny, I. 1990, ApJ, 361, 320

Caffee, M., Hohenberg, C., & Swindle, T. 1987, ApJ, 313, L31

Canuto, V. M., Levine, J. S., Augustsson, T. R., Imhoff, C. L., & Giampapa, M. S. 1983, Nature, 305, 281

Carr, M. H. 1996, Water on Mars (Oxford Univ. Press: New York)

Charbonnel, C., Vauclair, S., & Zahn, J.-P. 1992, A&A, 255, 191

Cogley, J. G., & Henderson-Sellers, A. 1984, Rev. Geophys. Space Phys., 22, 131

Cohen, E. R., & Taylor, B. N. 1986, Codata Bulletin No. 63 (New York: Pergamon)

Crowley, T. J., & Berner, R. A. 2001, Science, 292, 870

Däppen, W., Mihalas, D., Hummer, D. G., & Mihalas, B. 1988, ApJ, 332, 261

Eiler, J. M., Mojzsis, S. J., & Arrhenius, G. 1997, Nature, 386, 665

Eriksson, K. A. 1982, Tectonophysics, 81, 179

Gaidos, E. J., Güdel, M., & Blake, G. A. 2000, Geophys. Res. Lett., 27, 501

Geiss, J. 1973, in Proc. 13th Intl. Cosmic Ray Conf., vol. 5 (Denver: Univ. of Denver), 3375

Geiss, J., & Bochsler, P. 1991, in The Sun in Time, ed. C. Sonnett, M. Giampapa, & M. Matthews (Tucson: Univ. Arizona Press), 98

Goldspiel, J., & Squyres, S. W. 1991, Icarus, 89, 392

Grevesse, N., & Noels, A. 1993, in Origin and Evolution of the Elements, ed. N. Prantzos, E. Vangioni-Flam, & M. Cassé (Cambridge: Cambridge University Press), 15

Grevesse, N., & Sauval, A. J. 1998, Space Sci. Rev., 85, 161

Gruzinov, A. V., & Bahcall, J. N. 1997, ApJ, 490, 437

Gruzinov, A. V., & Bahcall, J. N. 1998, ApJ, 504, 996

Guenther, D. B., Demarque, P., Kim, Y.-C., & Pinsonneault, M. H. 1992, ApJ, 387, 372

Guzik, J. A., & Cox, A. N. 1995, ApJ, 448, 905

Guzik, J. A., Willson, L. A., & Brunish, W. M. 1987, ApJ, 319, 957

Hobbs, L. M., & Pilachowski, C. 1988, ApJ, 334, 734

Holland, H. D., Lazar, B., & McCaffrey, M. 1986, Nature, 320, 27

Iglesias, C. A., & Rogers, F. J. 1996, ApJ, 464, 943

Karhu, J., & Epstein, S. 1986, Geochim. Cosmochim. Acta, 50, 1745

Kasting, J. 1982, J. Geophys. Res., 87, 3091

Kasting, J. 1988, Icarus, 74, 472

Kasting, J. 1989, Palaeogeogr. Palaeoclimat. Palaeocol., 75, 83

Kasting, J. 1991, Icarus, 94, 1

Kasting, J., & Ackerman, T. P. 1986, Science, 234, 1383

Kasting, J. F., Whitmire, D. P., & Reynolds, R. T. 1993, Icarus, 101, 108

Kerridge, J. F., Signer, P., Wieler, R., Becker, R. H., & Pepin, R. O. 1991, in The Sun in Time, ed. C. Sonnett, M. Giampapa, & M. Matthews (Tucson: Univ. Arizona Press), 389

Knauth, L. P., & Epstein, S. 1976, Geochim. Cosmochim. Acta, 40, 1095

Kuhn, W. R., & Kasting, J. F. 1983, Nature, 301, 53

Kuhn, W. R., Walker, J. C. G., & Marshall, H. G. 1989, J. Geophys. Res., 94, 11129

Lebreton, Y., & Maeder, A. 1987, A&A, 175, 99

Lovelock, J. 1988, The Ages of Gaia (Norton: London), chap. 4

Mojzsis, S. J., Arrhenius, G., McKeegan, K. D., Harrison, T. M., Nutman, A. P., & Friend, C. R. L. 1996, Nature, 384, 55; —. 1997, Nature, 386, 738 (Erratum)

Morel, P., Provost, J., & Berthomieu, G. 1997, A&A, 327, 349

North, G. R. 1975, J. Atmos. Sci., 32, 2033

Nutman, A. P., Allaart, J. H., Bridgwater, D., Dimroth, E., & Rosing, M. 1984, Precambrian Res., 25, 365

Oberbeck, V. R., Marshall, J. R., & Aggarwal, H. R. 1993, J. Geol., 101, 1

Ohmotu, H., & Felder, R. P. 1987, Nature, 328, 244

Parker, T. J., Gorsline, D. S., Saunders, R. S., Pieri, D. C., & Schneeberger, D. M. 1993, J. Geophys. Res., 95, 11061

Pinsonneault, M. H., Kawaler, S. D., Sofia, S., & Demarque, P. 1989, ApJ, 338, 424

Pollack, J. B. 1979, Icarus, 37, 479

Pollack, J. B., Kasting, J. F., Richardson, S. M., & Poliakoff, K. 1987, Icarus, 71, 203

Ragas, K., & Pollack, J. B. 1980, Icarus, 41, 119

Retallack, G. J. 2001, Nature, 411, 287

Richard, O., Vauclair, S., Charbonnel, C., & Dziembowski, W. A. 1996, ApJ, 312, 1000

Rogers, F. J., Swenson, F. J., & Iglesias, C. A. 1996, ApJ, 456, 902

Rye, R., Kuo, P. H., & Holland, H. D. 1995, Nature, 378, 603

Sackmann, I.-J., Boothroyd, A. I., & Kraemer, K. E. 1993, ApJ, 418, 457

Sagan, C. 1977, Nature, 269, 224

Sagan, C., & Chyba, C. 1997, Science, 276, 1217

Sagan, C., & Mullen, G. 1972, Science, 177, 52

Salpeter, E. E. 1955, ApJ, 121, 161

Schaefer, M. W. 1990, J. Geophys. Res., 95, 14291

Schatzman, E. 1977, A&A, 56, 211

Squyres, S. 1993, MSATT LPI Workshop on Early Mars: How Warm and How Wet?, LPI Tech. Report No. 93-03, Part 1

Swenson, F. J., & Faulkner, J. 1992, ApJ, 395, 654

Swenson, F. J., Faulkner, J., Iglesias, C. A., Rogers, F. J., & Alexander, D. R. 1994, ApJ, 422, L79

Thoul, A. A., Bahcall, J. N., & Loeb, A. 1994, ApJ, 421, 828

Ulrich, R. K., & Rhodes, E. R., Jr. 1983, ApJ, 265, 551

Walker, J. C. G., Hays, P. B., & Kasting, J. F. 1981, J. Geophys. Res., 86, 9776

Wang, W. C., & Stoner, P. H. 1980, J. Atmos. Sci., 37, 545

Whitmire, D. P., Doyle, L. R., Reynolds, R. T., & Matese, J. J. 1995, J. Geo. Res. Planets, 100, 5457

Willson, L. A., Bowen, G. H., & Struck-Marcel, C. 1987, Comm. Ap., 12, 17

Woese, C. 1987, Microbiol. Rev., 51, 221

Wood, B. E., & Linsky, J. L. 1998, ApJ, 492, 788

Wood, B. E., Linsky, J. L., Müller, H.-R., & Zank, G. P. 2001, ApJ, 547, L49

Yung, Y. L., Nair, H., & Gerstell, M. F. 1997, Icarus, 130, 222

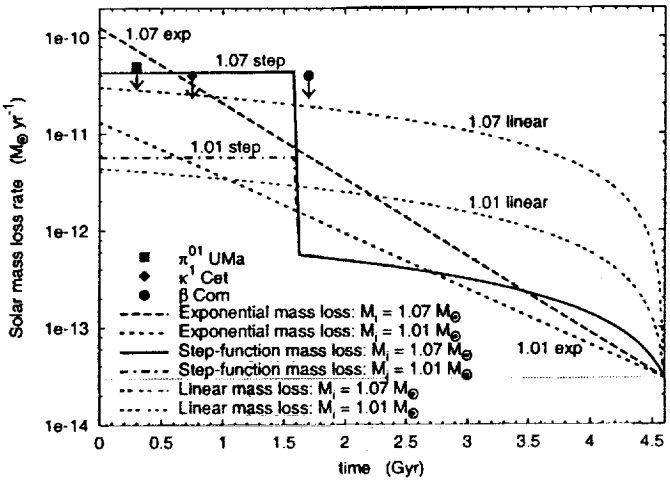

Fig. 1.— Mass loss rates as a function of time for our "exponential," "step-function," and "linear" solar mass loss cases. The lowest and the highest mass loss cases that we considered are shown (M_i = 1.01 and 1.07 $M_\odot$, respectively). Mass loss upper limits for the young Sun-like stars π^{01} UMa, κ^1 Cet, and β Com are from Gaidos et al. (2000).

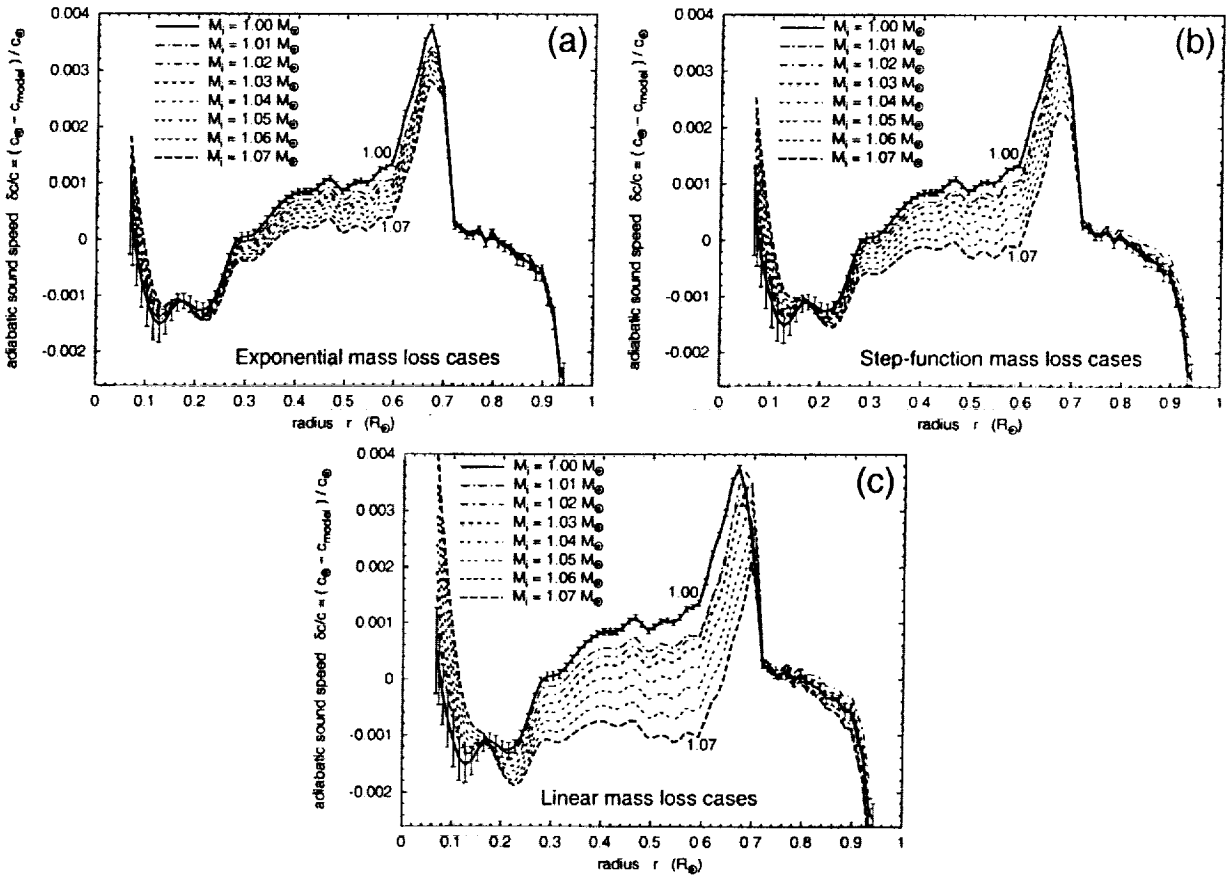

Fig. 2.— The effects of mass loss on the adiabatic sound speed c for (a) exponential, (b) step-function, and (c) linear mass loss cases. The *heavy solid line* is the reference standard solar model (no mass loss); the errorbars give the statistical error in the inferred helioseismic profile.

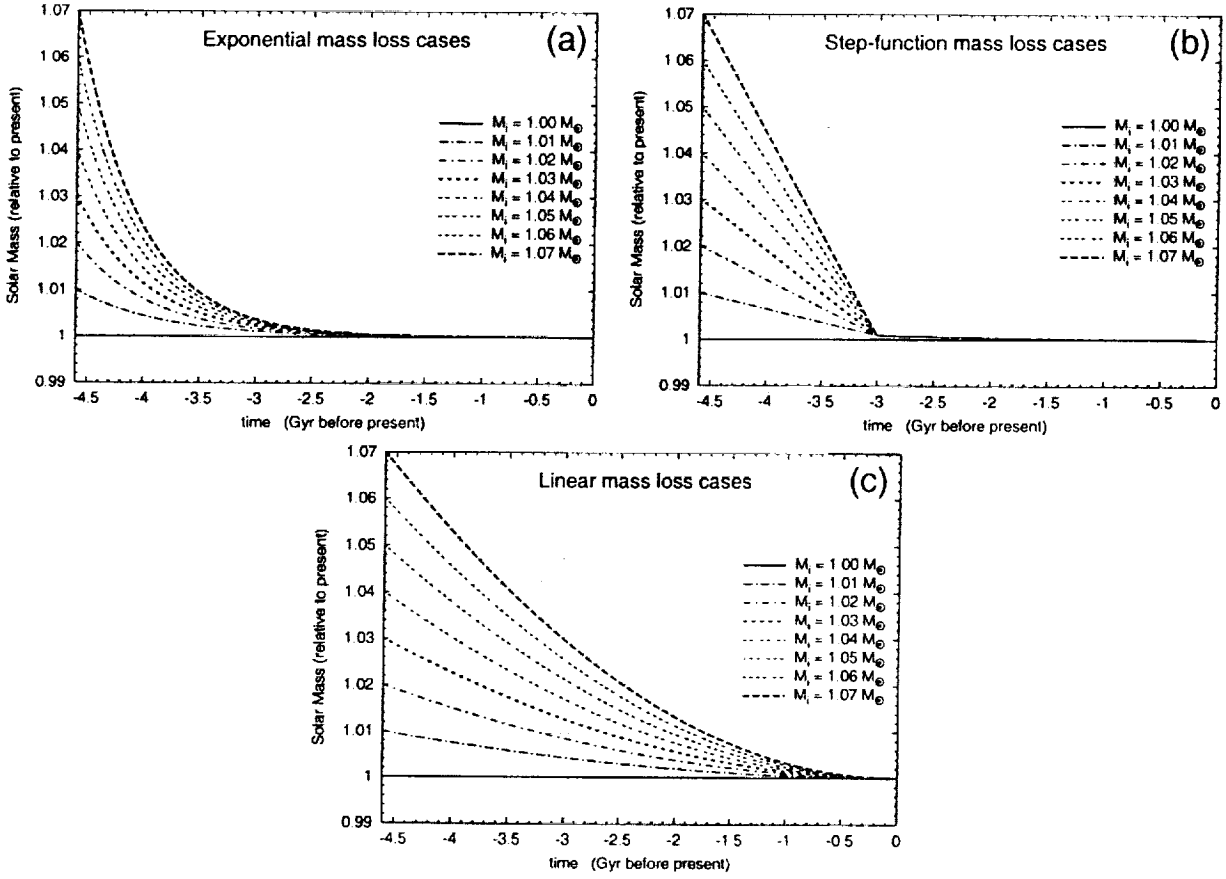

Fig. 3.— Solar mass as a function of time for (a) exponential, (b) step-function, and (c) linear mass loss cases.

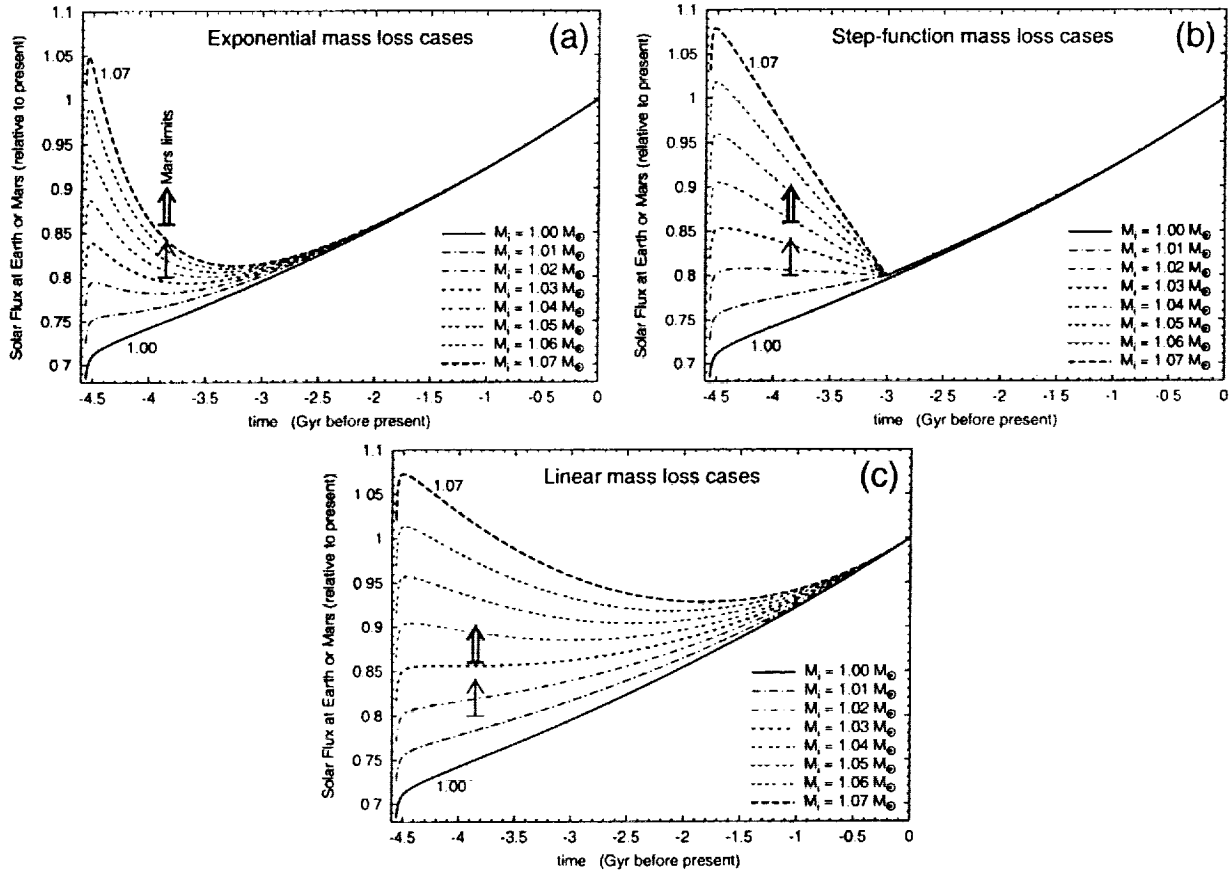

Fig. 4.— Solar flux at the planets as a function of time (relative to the present flux), for (a) exponential, (b) step-function, and (c) linear mass loss cases. Heavy double arrows give the lower flux limit of Kasting (1991) for the presence of water on early Mars; light single arrows give his extreme lower flux limit (for a model with an unrealistically low Martian surface albedo).

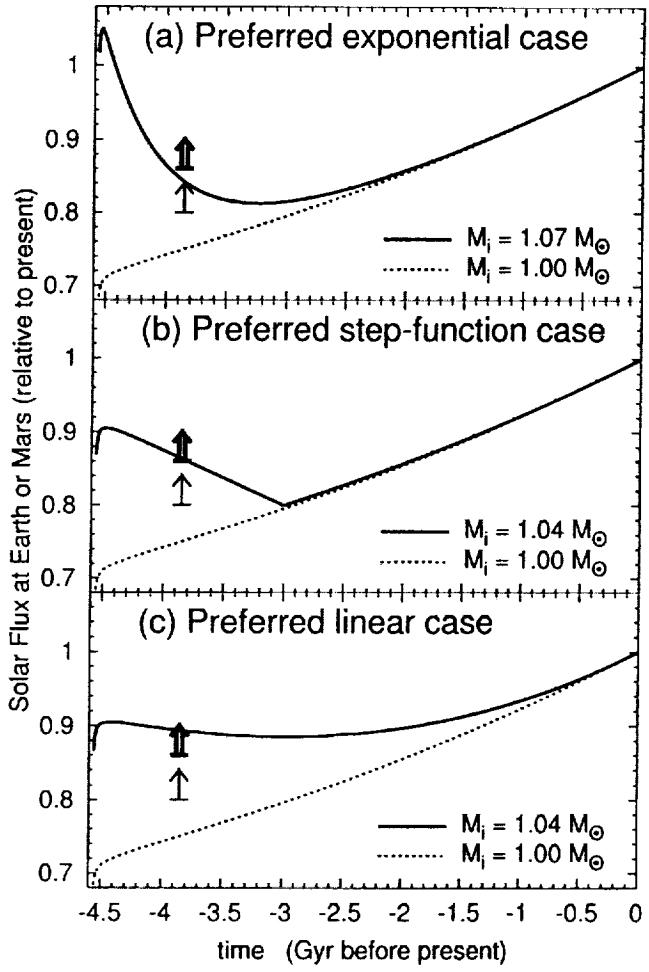

Fig. 5.— Solar flux at the planets (relative to the present flux) as a function of time for our preferred initial masses, for each type of mass loss that we considered. Heavy double arrows give the lower flux limit of Kasting (1991) for the presence of water on early Mars; light single arrows give his extreme lower flux limit (for a model with an unrealistically low Martian surface albedo).

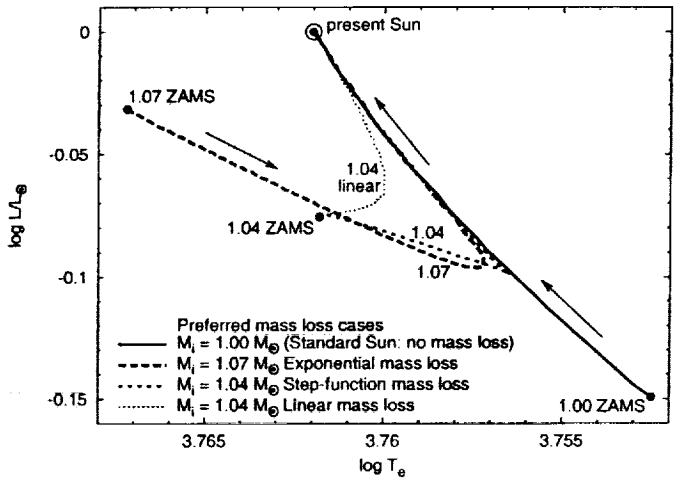

Fig. 6.— Evolution in the H-R diagram of the standard solar model, and of our preferred mass loss cases for each type of mass loss considered. The "ZAMS" points shown are actually $\sim$ 50 Myr subsequent to the start of nuclear burning on the main sequence, i.e., the rapid loop due to initial CN-cycle burning is omitted for clarity.

Table 1. Characteristics of Our Solar Models[a]

Solar Model	α	Z_0	Y_0	Y_e	R_{ce} ($R_\odot$)	rms $\delta c/c$ for: all-r	rms $\delta c/c$ for: < 0.6	rms $\delta\rho/\rho$	relative rms vs.	relative rms $\Delta c/c$	relative rms $\Delta\rho/\rho$	f_{Li}	f_{Be}	Φ_{Cl}	Φ_{Ga}	Φ_B
1. Fine-zoned Reference[b]	1.817	.02030	.2760	.2424	.7135	.00133	.00085	.01698		...	...	24.24	1.008	7.87	133.7	5.31
2. Fine-zoned 1.01 $M_\odot$ exp	1.818	.02025	.2754	.2425	.7133	.00116	.00074	.01533	1	.00028	.00179	19.22	1.009	7.87	133.7	5.32
3. Fine-zoned 1.02 $M_\odot$ exp	1.819	.02017	.2748	.2425	.7133	.00126	.00074	.01544	1	.00017	.00158	17.43	1.009	7.87	133.7	5.32
4. Fine-zoned 1.03 $M_\odot$ exp	1.819	.02012	.2743	.2426	.7133	.00118	.00070	.01437	1	.00034	.00276	17.81	1.009	7.88	133.7	5.32
5. Fine-zoned 1.04 $M_\odot$ exp	1.819	.02007	.2738	.2427	.7132	.00118	.00068	.01398	1	.00034	.00311	19.91	1.012	7.89	133.8	5.33
6. Fine-zoned 1.05 $M_\odot$ exp	1.821	.02003	.2734	.2428	.7131	.00112	.00065	.01340	1	.00039	.00366	22.96	1.026	7.91	133.9	5.35
7. Fine-zoned 1.06 $M_\odot$ exp	1.821	.01999	.2730	.2428	.7130	.00105	.00063	.01247	1	.00049	.00464	26.99	1.069	7.92	133.9	5.35
8. Fine-zoned 1.07 $M_\odot$ exp	1.823	.01997	.2726	.2429	.7128	.00096	.00062	.01162	1	.00060	.00550	31.82	1.173	7.94	134.1	5.37
9. Coarse-zoned Reference[b,c]	1.814	.02030	.2760	.2424	.7136	.00140	.00091	.01772	1[c]	.00008	.00074	24.36	1.010	7.89	133.8	5.33
10. 1.01 $M_\odot$ exp	1.816	.02024	.2754	.2427	.7134	.00128	.00081	.01641	9	.00016	.00134	19.22	1.009	7.91	134.0	5.35
11. 1.02 $M_\odot$ exp	1.816	.02016	.2748	.2429	.7134	.00124	.00077	.01569	9	.00024	.00208	17.26	1.009	7.89	133.8	5.33
12. 1.03 $M_\odot$ exp	1.816	.02010	.2742	.2431	.7134	.00120	.00074	.01515	9	.00030	.00263	17.82	1.009	7.89	133.8	5.33
13. 1.04 $M_\odot$ exp	1.816	.02005	.2738	.2433	.7133	.00115	.00070	.01448	9	.00037	.00332	19.72	1.012	7.90	133.8	5.34
14. 1.05 $M_\odot$ exp	1.817	.02001	.2734	.2433	.7133	.00111	.00067	.01379	9	.00045	.00402	22.82	1.026	7.91	133.9	5.35
15. 1.06 $M_\odot$ exp	1.818	.01997	.2730	.2434	.7131	.00105	.00065	.01300	9	.00053	.00484	27.47	1.068	7.93	134.0	5.36
16. 1.07 $M_\odot$ exp	1.819	.01995	.2726	.2434	.7131	.00101	.00063	.01217	9	.00062	.00569	34.25	1.170	7.95	134.1	5.38
17. 1.01 $M_\odot$ step	1.816	.02019	.2751	.2426	.7134	.00128	.00080	.01626	9	.00018	.00149	19.57	1.009	7.87	133.7	5.32
18. 1.02 $M_\odot$ step	1.815	.02007	.2742	.2432	.7135	.00124	.00077	.01572	9	.00027	.00204	18.94	1.009	7.86	133.6	5.31
19. 1.03 $M_\odot$ step	1.815	.01999	.2734	.2435	.7135	.00117	.00072	.01463	9	.00035	.00316	20.87	1.011	7.88	133.7	5.32
20. 1.04 $M_\odot$ step	1.816	.01993	.2728	.2437	.7133	.00109	.00067	.01347	9	.00048	.00435	24.36	1.025	7.90	133.8	5.34
21. 1.05 $M_\odot$ step	1.818	.01988	.2722	.2437	.7131	.00101	.00064	.01207	9	.00063	.00580	29.75	1.074	7.94	134.0	5.37
22. 1.06 $M_\odot$ step	1.821	.01985	.2716	.2437	.7129	.00095	.00064	.01061	9	.00079	.00733	37.76	1.213	7.98	134.3	5.40
23. 1.07 $M_\odot$ step	1.823	.01982	.2711	.2436	.7126	.00089	.00068	.00916	9	.00095	.00883	49.63	1.534	8.01	134.4	5.43
24. 1.01 $M_\odot$ linear	1.818	.02021	.2749	.2427	.7132	.00116	.00070	.01486	9	.00035	.00293	19.70	1.009	7.94	134.1	5.37
25. 1.02 $M_\odot$ linear	1.818	.01997	.2731	.2429	.7131	.00122	.00069	.01427	9	.00046	.00356	18.49	1.009	7.92	134.0	5.36
26. 1.03 $M_\odot$ linear	1.816	.01972	.2713	.2439	.7133	.00115	.00069	.01293	9	.00060	.00496	20.11	1.011	7.87	133.6	5.32
27. 1.04 $M_\odot$ linear	1.817	.01959	.2700	.2445	.7133	.00105	.00070	.01084	9	.00082	.00713	23.34	1.027	7.90	133.8	5.35
28. 1.05 $M_\odot$ linear	1.817	.01947	.2687	.2450	.7132	.00099	.00078	.00858	9	.00106	.00958	28.35	1.081	7.95	134.1	5.38
29. 1.06 $M_\odot$ linear	1.821	.01937	.2675	.2452	.7128	.00099	.00094	.00640	9	.00132	.01200	36.71	1.250	8.00	134.4	5.43
30. 1.07 $M_\odot$ linear	1.824	.01929	.2663	.2452	.7125	.00108	.00114	.00432	9	.00161	.01476	48.90	1.631	8.07	134.7	5.48
31. GS98 reference[d]	1.787	.01911	.2758	.2419	.7157	.00192	.00122	.02125	9[d]	.00056	.00373	22.60	1.009	7.76	132.8	5.26
32. GS98 1.01 $M_\odot$ exp	1.776	.01906	.2752	.2421	.7154	.00178	.00111	.02014	31	.00035	.00123	14.85	1.008	7.78	132.9	5.28
33. GS98 1.02 $M_\odot$ exp	1.776	.01899	.2746	.2422	.7154	.00175	.00105	.01929	31	.00035	.00201	13.70	1.008	7.72	132.5	5.23
34. GS98 1.03 $M_\odot$ exp	1.776	.01893	.2741	.2425	.7153	.00168	.00101	.01864	31	.00044	.00267	14.47	1.008	7.73	132.6	5.24
35. GS98 1.04 $M_\odot$ exp	1.777	.01889	.2736	.2427	.7153	.00162	.00097	.01799	31	.00049	.00332	16.46	1.010	7.74	132.6	5.25
36. GS98 1.05 $M_\odot$ exp	1.778	.01885	.2732	.2428	.7152	.00157	.00092	.01725	31	.00056	.00407	19.58	1.025	7.75	132.7	5.26

Table 1—Continued

Solar Model	α	Z_0	Y_0	Y_e	R_{ce} ($R_\odot$)	rms $\delta c/c$ for: all-r	rms $\delta c/c$ for: < 0.6	rms $\delta\rho/\rho$	relative rms vs.	relative rms $\Delta c/c$	relative rms $\Delta\rho/\rho$	f_{Li}	f_{Be}	Φ_{Cl}	Φ_{Ga}	Φ_B
37. GS98 1.06 $M_\odot$ exp	1.778	.01881	.2728	.2428	.7151	.00152	.00088	.01652	31	.00063	.00481	24.15	1.062	7.77	132.7	5.27
38. GS98 1.07 $M_\odot$ exp	1.780	.01879	.2724	.2428	.7150	.00145	.00084	.01573	31	.00070	.00561	30.84	1.160	7.78	132.8	5.28

[a] Mixing length parameter α, pre-solar metallicity Z_0 and helium mass fraction Y_0, present envelope helium abundance Y_e, position R_{ce} of the base of envelope convection, rms fractional sound speed and density differences relative to the Sun's inferred helioseismic profiles and relative to the reference standard solar model, pre-main-sequence lithium depletion factor f_{Li} and beryllium depletion factor f_{Be}, predicted capture rates (in SNU) ϕ_{Cl} and ϕ_{Ga} for chlorine and gallium experiments, respectively, and predicted flux ϕ_B of ^{8}B neutrinos (in units of 10^6 cm s^{-1}). Seven different cases with initial masses from 1.01 to 1.07 $M_\odot$ are shown for each of the three mass loss types, namely, exponential ("exp"), step-function ("step"), and linear ("linear").

[b] Reference standard solar model: OPAL EOS at $\log\rho \gtrsim -1.5$, MHD EOS at $\log\rho \lesssim -2$, high-T opacities $\kappa_{\rm OPAL:GN93}$ interpolated in $Z_\kappa = Z_h \equiv Z_0[\sum_{heavy} X_i]/[\sum_{heavy}(X_i)_0]$ as well as in "excess" C and O (such that $C_{ex} + O_{ex} \equiv CO_{ex} = Z - Z_\kappa$), low-T opacities $\kappa_{\rm Alexander}$, NACRE nuclear rates, gravitational settling of He and heavy elements, $Z/X = 0.0245$, $L_\odot = 3.854 \times 10^{33}$ erg s^{-1}, $R_\odot = 695.98$ Mm, and $t_\odot = 4.6$ Gyr; both fine-zoned and coarse-zoned cases were computed.

[c] This reference standard solar model and all subsequent models in the table use the coarse zoning. Note that the relative rms values for this coarse-zoned reference standard solar model compare it to the fine-zoned reference model.

[d] This "GS98" alternate standard solar model (and the following "GS98" mass-losing models in the table) has $Z/X = 0.023$ with the appropriate OPAL opacities $\kappa_{\rm OPAL:GS98}$, using the OPAL EOS at $\log T \gtrsim 4.0$ and the MHD EOS at $\log T \lesssim 3.9$; otherwise it is the same as the coarse-zoned reference standard solar model. The relative rms values for this "GS98" alternate standard solar model compare it to the coarse-zoned reference model.